X-ray structural determination of the quasi-commensurate phase of barium sodium niobate

1990 J. Phys.: Condens. Matter 2 25

(http://iopscience.iop.org/0953-8984/2/1/002)

J. Phys.: Condens. Matter **2** (1989) 25–43. Printed in the UK

X-ray structural determination of the quasi-commensurate phase of barium sodium niobate

Ph Labbé†, H Leligny†, B Raveau†, J Schneck‡ and J C Tolédano‡

† Laboratoire CRISMAT, ISMRa, Bd du Maréchal Juin, 14032 Caen Cédex, France

‡ Laboratoire de Bagneux, CNET, 196 rue de Paris, 92220 Bagneux, France

Received 15 December 1988, in final form 17 July 1989

Abstract. In order to provide an accurate basis for the interpretation of the physical properties of this complex incommensurate system, the structure of the room temperature quasi-commensurate phase of barium sodium niobate is determined by taking into account, for the first time, the satellite reflections present in the diffraction spectrum of this material. The quasi-commensurate phase considered is assimilated to a strictly commensurate phase, the satellite reflections being considered as superlattice reflections and referred to a crystalline supercell with $a = 35.187$ Å, $b = 17.620$ Å and $c = 7.987$ Å. This approximation gives an excellent agreement index $R = 0.031$ for the fit to the intensities of the 2432 basic reflections and the 1691 satellite reflections collected at 294 K (λMo $K\alpha = 0.71069$ Å, $\mu_l = 111.47$ cm^{-1}, space group: B*b*m2). The structural results show that the commensurate modulation consists of a tilting and a shearing of all the NbO_6 octahedra in the structure in contrast to previous inferences which had only suggested the occurrence of a shear. The framework of the structure may be described on the basis of the existence of two different Nb_5O_{24} units of five corner-sharing octahedra each. The structure obtained by spatially averaging the modulation is consistent with previous structural studies of the basic reflections of this material. Physical characteristics pertaining to the polar character, or the domain structure, are also deduced.

1. Introduction

Barium sodium niobate (BNN) has been the subject of extensive physical investigations in the last 20 years. The main motivations for these studies was the occurrence in this material of a number of phase transitions [1] and the existence of incommensurate phases with many peculiar features [2]. In particular, BNN is one of the few known structural systems in which one can have several distinct incommensurate phases differing by the number of directions of the modulations [3]. Also, it is a system in which the interaction of the incommensurate modulation with structural defects produces exceptionally large observable effects [4].

A number of experimental techniques have been used to clarify the nature of the incommensurability and the mechanism of the phase transitions: x-ray precession studies as a function of the temperature [2], static and dynamic neutron scattering [5], optical measurements [6] and electron microscopic observations in direct and reciprocal space [7].

However, up to now, the interpretation of the data obtained from the various experiments has rested on uncertain structural information. This information was based

0953-8984/90/010025 + 19 $03.50

partly on theoretical speculations, partly on x-ray precession data [5] and partly on a structure determination by Jamieson *et al* [8] who had worked out a spatially averaged atomic arrangement for the structure of BNN but not its actual modulated atomic configuration.

In view of the importance of this system to the understanding of complex incommensurate systems, it would be of great interest to elucidate the complete structure of BNN, by taking effectively into account the existence of the superlattice reflections associated with a modulation of the atomic positions.

In this paper, we present the results of such a refinement of the structure of BNN at room temperature.

The difficulty in determining this structure, pertains to the fact that, below 300 °C, all the phases of BNN are incommensurate, the degree of deviation from commensurability being more or less pronounced. In order to perform a structure determination, by means of standard methods, we have taken advantage of the fact that, at room temperature, the deviation from commensurability is very small [2], and that it is possible to describe satisfactorily the structure by assigning to it an approximate unit cell of reasonable size.

2. Available structural data

At room temperature, the atomic coordinates determined by Jamieson *et al* [8] correspond to a slightly distorted tetragonal tungsten bronze structure [9], having the symmetry Cmm2. This result provides only some averaged structure of BNN, since the preceding structural determination does not incorporate the superlattice reflections subsequently discovered in the x-ray diffraction spectrum of BNN. The reflections considered by Jamieson *et al* are the reflections of the regular tungsten bronze structure. They form the basic Bragg reflections of BNN.

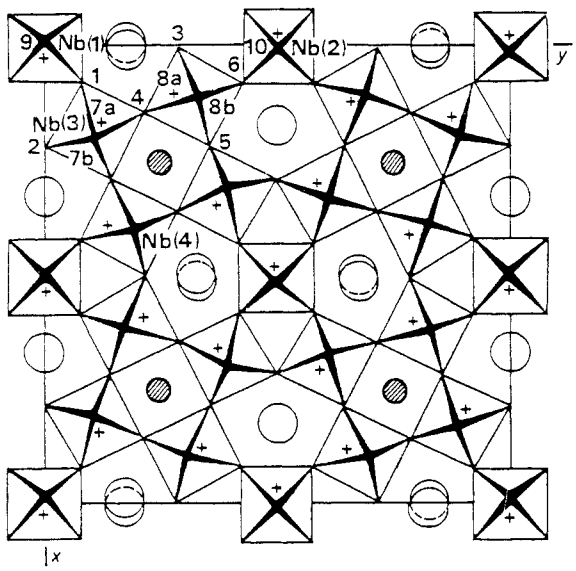

Figure 1. Projection (001) of the mean structure of BNN according to [8].

In order to describe the structure found by Jamieson *et al* (figure 1), it is of interest to refer to the regular tetragonal tungsten bronze structure, which is believed to be realised, for BNN, in the range of temperatures above 585 °C. This structure, of symmetry P4/m*b*m, is constituted by corner-sharing NbO_6 octahedra forming three types of cages, one of which, triangular shaped, is empty, and the two others, respectively cubic and pentagonal, are occupied by sodium and barium cations. The lattice constants of this reference structure are $a_t = b_t \sim 12.4$ Å, and $c_t \sim 4$ Å.

The orthorhombic cell determined by Jamieson *et al* for the room temperature structure of BNN is turned by 45° around the *c*-axis with respect to the preceding tetragonal cell. The lattice constants are $a_0 \sim b_0 \sim 17.6$ Å and $c_0 \sim 4$ Å, the relative difference between a_0 and b_0 being of the order of 10^{-3}. The cubic, perovskite-like cages, are statistically occupied by Na and Ba, the latter cations being in small proportions. The polar axis is parallel to $\boldsymbol{c}$, in agreement with displacements along this axis of the Nb cations out of the centres of the octahedra. It is worth pointing out that, due to the existence of a tetragonal P4/m*b*m pseudo-symmetry of the structure, BNN samples will generally contain domains of two types. One type of twinning corresponds to the reversal of the polar axis, which gives rise to ferroelectric domains differing by the sense of a spontaneous polarisation. The other type of twinning corresponds to the interchange of the $\boldsymbol{a}$- and $\boldsymbol{b}$-axes, which gives rise to ferroelastic domains. In order to avoid generating an erroneous pseudo-symmetry in the investigated sample, Jamieson *et al* worked on a single domain sample, which they obtained by detwinning a crystal electrically and mechanically.

One of the most interesting features of the structure described by Jamieson *et al* (figure 1) is their observation of pairs of split positions for some Ba atoms as well as for all the oxygen atoms located in the plane $z = 0.5$. A given 'split' atom occupies the two positions in a pair with probability one half. More recent physical and crystallographical studies have reinterpreted this splitting, and assigned to it a central role in the mechanism of the superstructure of BNN [1, 2, 5, 7]. These studies have shown that, at room temperature, superlattice spots exist at positions in reciprocal space which are specified, with respect to the basic Bragg reflections, by the vectors $\pm[\frac{1}{4}(\boldsymbol{a}_t^* + \boldsymbol{b}_t^*)(1 + \delta) + \frac{1}{2}\boldsymbol{c}_t^*]$ or, equivalently, by the vectors $\pm[\frac{1}{2}\boldsymbol{a}_0^*(1 + \delta) + \frac{1}{2}\boldsymbol{c}_0^*]$. The incommensurability parameter δ is of the order of 1%. Neglecting this small value, we can see that the superstructure associated with the former spots corresponds to an orthorhombic cell twice as large as the Jamieson unit cell along $\boldsymbol{a}_0$ and along $\boldsymbol{c}_0$. Taking into account the superlattice reflections, it has been possible to assign the B*b*m2 space group to the room temperature structure of BNN. Theoretical speculations [5] have assigned the above splitting of atomic positions to the averaging within the reduced Jamieson unit cell of the positions of distinct atoms of the actual unit cell. Up to now, no substantiation of this assignment, by means of a structural determination, has been given, though some support has been obtained using high-resolution electron microscopic observations in real space [7].

3. Experimental

3.1. Preparation and preliminary tests

Crystals were grown by pulling them from a stoichiometric melt using the Czochralski technique. Radiochemical analysis, using neutron activation, yielded for the selected

crystal the composition $Ba_{4.17}Na_{1.67}Nb_{10}O_{30}$, in good agreement with the results of the refinements of the structure.

The as-grown crystal was electrically polarised in order to make it a single ferroelectric domain. In this view a standard procedure was used, that involved heating the sample, which was provided with silver paste electrodes on the *c*-faces, to above the ferroelectric transition, applying a suitable electric field (corresponding to the flow of ~1 mA through the crystal) and then maintaining this field during the cooling of the sample down to room temperature.

Twelve samples of about cubic shape of dimensions from 100 to 200 μm were cut from the previously prepared crystal. This shape, which allows us to take the absorption correction easily into account, was preferred to a ground sphere because it does not include powder traces on the surface. The crystals were all tested in a Weissenberg camera, as well as by the rotating-crystal method around the *c*-axis. Zero and upper Weissenberg levels showed that most of the crystals contained ferroelastic domains. These can easily be detected on the films by searching for a splitting of the basic Bragg spots at high angle (except those relative to the rows $[hhl]^*$ which remain unmodified by the interchange of $\boldsymbol{a}$ and $\boldsymbol{b}$ axes).

However, two crystals among the twelve appeared as single-domain ferroelastic samples since they presented no detectable splitting of the basic reflections and no clear evidence of an additional array of reflections in the superlattice levels. One of them, which displayed sharp spots, was selected for the data collection. A more accurate estimation of its degree of twinning is described in § 3.2. Note that, in agreement with the results of Schneck and Denoyer [2], the diffraction patterns obtained in these Weissenberg photographs appear consistent with the lattice constants $a = 2a_0$, $b = b_0$ and $c = 2c_0$, and with the space group B*b*m2.

3.2. Data collection

The intensities of 4123 independent reflections were collected with a CAD4 Enraf-Nonius diffractometer. The main features of the data collection and reduction are summarised in table 1. All these reflections, collected with reference to the large orthorhombic cell defined below (a, b, c), have been classified into three families (figure 2):

(*a*) 2432 basic reflections denoted by BR, corresponding to $l = 2n$; $h = 4n$ and $k = 2n$; or $h = 4n + 2$ and $k = 2n + 1$ (figure 2(*a*)).

(*b*) 122 superstructure reflections denoted by SR1, all of very weak intensities, and corresponding to $l = 2n$; $h = 4n$ and $k = 2n + 1$; or $h = 4n + 2$ and $k = 2n$ (figure 2(*a*)).

(*c*) 1569 superstructure reflections denoted by SR2, of weak or medium intensities, corresponding to $l = 2n + 1$ and $h = 2n + 1$ without condition relative to k (figure 2(*b*)).

The weakness of the SR1 intensities denotes that the vector $(\frac{1}{4}\boldsymbol{a} + \frac{1}{2}\boldsymbol{b})$ is an approximate lattice vector for the structure. By contrast, the occurrence of the SR2 reflections with significant intensity denote that $\frac{1}{2}\boldsymbol{c}$ is not a good lattice vector.

In order to complete the corrections of the raw data, we have undertaken a series of additional measurements aimed at specifying a possible residual twinning into ferroelastic domains.

It can be noted on figure 2(*a*) that, if an interchange of the $\boldsymbol{a}$ and $\boldsymbol{b}$ axes is effected, the points hkl and $(2k, \frac{1}{2}h, l)$ with $l = 2n$, corresponding respectively to the two different orientations, are almost superimposed on either sides of the plane $(1\bar{2}0)_0^*$, since $2a^*$ is

Table 1. Experimental data and structure refinement parameters.

Crystal shape and size	Orthorhombic sample limited by {100}, {010} and {001} ($136 \times 150 \times 150\ \mu m$)
Lattice parameters ($T = 294$ K)	$a = 35.1869(22)$, $b = 17.6202(18)$, $c = 7.9876(10)$ Å
Conditions limiting possible reflections	hkl, $h + l = 2n$; $0kl$, $k = 2n$ ($l = 2n$)
Polar space group	Bbm2
Data collection technique	Diffractometer CAD 4 Enraf–Nonius, ω–2θ scan, Mo Kα ($\lambda = 0.71069$ Å)
Max value of $\sin\theta/\lambda$	0.997
No of measured reflections	17333 ($-70 < h < 70$, $0 < k < 35$, $0 < l < 14$)
No of reflections used in the refinement ($I/\sigma(I) > 3$)	$n_{tot} = 4123$ Basic reflections $n_{BR} = 2432$ Superstr. refl. ($l = 2n$) $n_{SR1} = 122$ Superstr. refl. ($l = 2n + 1$) $n_{SR2} = 1569$
$R_{int} = \Sigma(I_0 - \langle I_0\rangle)/\Sigma I_0$	BR 0.022 SR1 0.037 SR2 0.032
Absorption correction applied	Based on the actual crystal morphology
Linear absorption coefficient	$\mu_l = 111.47\ cm^{-1}$
Transmission factors	$T_{min} = 0.221$ and $T_{max} = 0.324$
Atomic scattering factors (Nb^{5+}, Na^+, Ba^{2+}) f' and f'' values	*International Tables of X-ray Crystallography* [17]
Final conventional R	$R_{tot} = 0.031$ $R_w = 0.040$ $R_{BR} = 0.029$ $R_{SR1} = 0.067$ $R_{SR2} = 0.039$

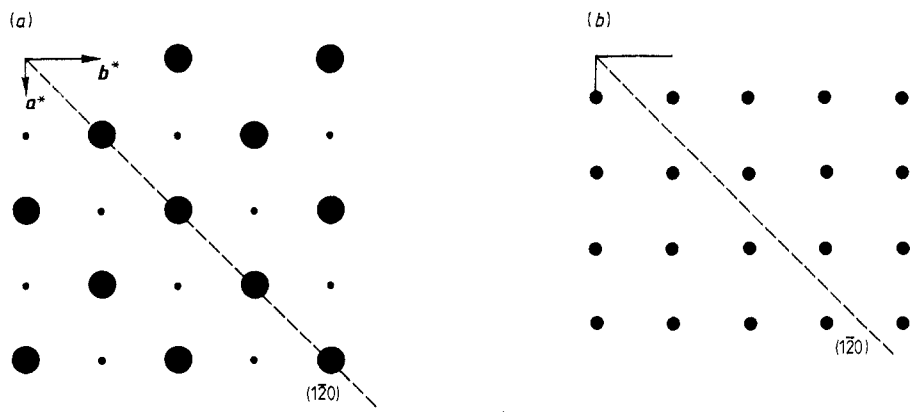

Figure 2. The three families of observed reflections. A hypothetical 90° domain leads to the mirror (1$\bar{2}$0) symmetry. (*a*), $h\,k\,2n$; (*b*), $h\,k\,2n + 1$.

nearly equal to b^*. This superposition will alter the reflections in the layers $l = 2n$. Their intensities can be corrected by using the method suggested by Britton [10] in the case of a twin. We have,

$$J_1 = I_1 + \frac{\alpha}{1-2\alpha}(I_1 - I_2) \qquad J_2 = I_2 - \frac{\alpha}{1-2\alpha}(I_1 - I_2)$$

where I and J are respectively the observed and corrected intensities, and where the subscripts 1 and 2 refer to the two possible domain orientations; α being the proportion of the minority orientation. Note that the reflections contained in the symmetry plane are not altered. Besides, it is established that the intensities I_1 and I_2 of the pairs of BR are nearly equal, on average: about half of the reflection pairs show differences in intensities $|I_1 - I_2| < 2(\sigma_1 + \sigma_2)$; σ_1 and σ_2 are the standard deviations relative to the two intensities I_1 and I_2 deduced from the counting statistics. Hence, the intensities are smoothly altered by the twinning.

Consider the results of the existence of ferroelastic domains on the $l = 2n + 1$ layers. In addition to the spots shown in figure 2(*b*), isolated extra spots should appear on each side of the (120)* plane, and the corrected values of the most intense reflections, $l = 2n + 1$, would be equal to $I_{obs}/(1 - \alpha)$.

In order to control the possible existence of residual domains in the sample considered, systematic intensity measurements have been performed in the $l = 1$ and $l = 3$ layers, by testing an interchange of the a^* and b^* parameters. We deduce from these measurements that extra spots are present and that their intensities are strongly correlated with those of the symmetric spots indicated in figure 2(*b*). In addition we were able to determine a value $\alpha = 0.07(1)$, assuming incoherent domains. All the collected intensities, I_0, were corrected from this twinning effect (I_{corr}). It is stated that the variances of I_{corr} and I_0 are of the same order of magnitude because for the BR, $I_1 \sim I_2$ and for the SR the estimated standard deviation (ESD) of α is negligible compared with the ESD of I_0 for most of the reflections. Then, it is to be expected that the ESDs of the resulting model are about those of a single-domain crystal.

All the collected intensities were corrected for the Lorentz factor, the polarisation and the absorption effects, on the basis of the known morphology of the sample.

The resulting values of the 4123 collected reflections were then used to solve and refine the structure of BNN.

4. Resolution of the structure†

Refining the atomic positions of such a complex structure involving 55 inequivalent atomic positions requires resorting to a structural model based on a preliminary knowledge of an approximate structure, as well as on additional geometrical considerations. We have performed this refinement in two steps. We have redetermined, first, the mean structure, and then taken into account the superstructure reflections in order to specify the complete structure.

† Additional material for this paper has been deposited with the British Library as supplementary publication SUP70039.

4.1. Structural model

In order to solve the mean structure, we consider first a simple model in which the NbO_6 octahedra constituting the skeleton of the structure are regular octahedra with O—O distances of the order of 2.80 Å (and, in any case, larger than 2.60 Å). This assumption contrasts with previous physical inferences [5, 7] which assumed a shearing of the octahedra as depicted in figure 3(*a*). This shearing was necessary to ensure the com-

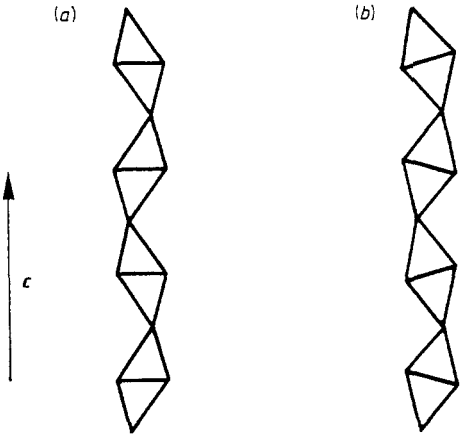

Figure 3. Shearing and tilting of a 001 chain of NbO_6 octahedra: (*a*) shearing according to [8]; (*b*), tilting according to this work.

patibility of the octahedral units with the distortions of the structure seen in figure 1. In our model, we ensure this compatibility by preserving the shape of the octahedra but by allowing for a rotation of each octahedron around an axis perpendicular to $\boldsymbol{c}$, and joining the middle of two opposite edges of the octahedron (cf figure 3(*b*)). An illustration of such a rotation is provided by the atoms O(7a) and O(7b) in figure 1.

Two consequences, relative to the mean structure, derive from our model.

(*a*) In both the shearing model and the rotation model, one expects that the O positions lying in the $z = 0.5$ plane will appear split when projected on the (001) plane of the mean structure. However, the rotation model only implies a similar splitting of the O positions lying in the $z = 0$ plane, when projected on a plane of the mean structure containing $\boldsymbol{c}$ (figure 3(*b*)).

(*b*) The set of rotations of the octahedra belonging to the different chains running along the $\boldsymbol{c}$-direction are not independent from one chain to another. There are constraints imposed by the symmetry and by the need to connect the chains to each other. Hence a small number of configurations are possible.

Once the mean structure is known, we have to generate the actual structure. In this view it is worth noting that the larger unit cell of the actual structure is generated from the cell of the mean structure by the four displacements associated with the vectors $\mathbf{0}$, $\frac{1}{2}\boldsymbol{c}$, $(\frac{1}{4}\boldsymbol{a} + \frac{1}{2}\boldsymbol{b})$ and $(\frac{1}{4}\boldsymbol{a} + \frac{1}{2}\boldsymbol{b} + \frac{1}{2}\boldsymbol{c})$. If identical atoms of the actual structure are situated at positions approximately related by one only of the non-zero preceding vectors, the mean structure will show a splitting of the corresponding atom into two positions. If the

positions in the actual structure are not approximately related by any of the above vectors, then the mean structure will show a splitting into four positions.

As an example, let us consider the perovskite cages for which one slice of four regular octahedra is drawn in figure 4. The tilting of an octahedron is limited to the type of rotation described above. We can see that there exist only three independent arrangements of the octahedra (figures 4(a, b, c)) in addition to the ones of the two slices above and below the one shown, which have not been represented since they correspond to opposite rotations. Note that the configuration 4(b) is not invariant under a 90° rotation while the configurations 4(a) and 4(c) are invariant. By translating the configurations 4(a) and 4(b) through the $\frac{1}{2}\boldsymbol{c}$, and by averaging the initial and translated configurations, we obtain respectively the configurations of figures 4(e) and 4(f) where the splitting of an oxygen into two positions is shown. Assume now that the two blocks considered are also in correspondence through the translation $\frac{1}{4}\boldsymbol{a} + \frac{1}{2}\boldsymbol{b}$, the averaging will lead to figure 4(g) where the oxygen atom is split into either two or four positions.

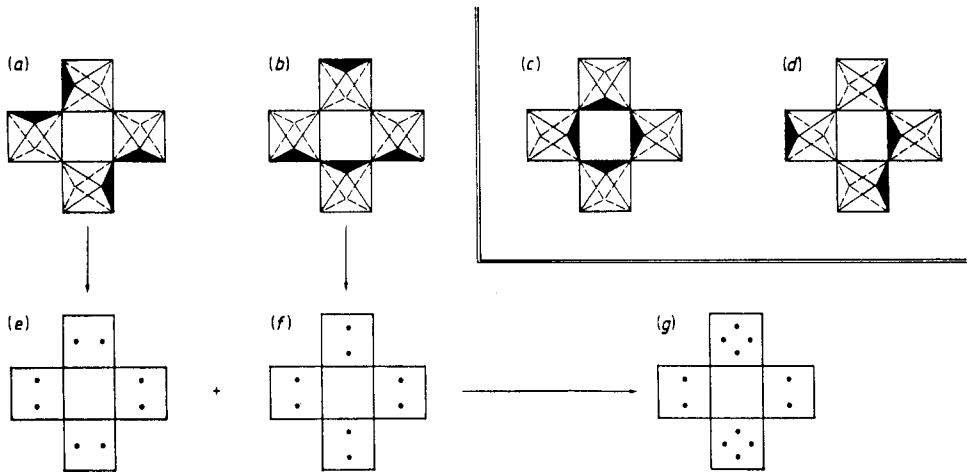

Figure 4. Arrangement of tilted NbO_6 octahedra in perovskite cages ((*a*) to (*d*)) and related splittings expected for the oxygen atoms in the mean structure ((*e*) to (*g*)). Through a [001] projection, the average of the two configurations (*a*) and (*b*) gives respectively the figures (*e*) and (*f*) where upper and lower oxygen atoms are split between two positions (dots). An average of the last two figures leads to the sketch (*g*), where oxygen atoms are split between two or four positions.

Though the preceding considerations pertain to the oxygen atoms in the octahedra, it must be noted that they are also valid for certain of the cations whose neighbourhood is modified by the octahedra rotations. This is mainly the case for barium atoms in the pentagonal cages, and secondarily for sodium atoms in the perovskite cages. No perturbation of the position of the niobium atoms is expected from the tilting in agreement with the structure refinement.

4.2. Refinement of the mean structure

A first test was made using only the 2432 BR. A refinement of the heavy atoms coordinates with βij anisotropic factors facilitated a systematic plot of the distribution of the elec-

tronic density around the expected positions of the oxygen sites using difference series calculations. The examples given (figures 5(*a*, *b*, *c*)) were encouraging because of their agreement with the previous hypothesis of two or four split oxygen positions. A refinement of all variables including the oxygen positions with the corresponding site occupation, and isotropic *B*-factors, resulted in conventional $R = 0.039$ and $R_w = 0.044$ (a_0, b_0, c_0, Cmm2). The scattering factor of the perovskite site was an average $f = 0.834f_{Na} + 0.0875f_{Ba}$ as deduced from the measured composition. The anomalous scattering factors $\Delta f'$ and $\Delta f''$ were introduced for all the atoms. The value z_0 of Nb(3) was fixed to determine the origin. The comparison of the resulting atomic positions with those given in [8] shows that all the x and y values of heavy atoms are the same within 2σ, whereas the z coordinates are distinct in a noticeable way. A difference mean value of $\langle \Delta z \rangle = 0.01$ Å is observed, the maximum value of $\Delta z = 0.04$ Å arising for an Na atom. For the oxygen atoms, the comparison is not more suitable in view of their splitting within this work.

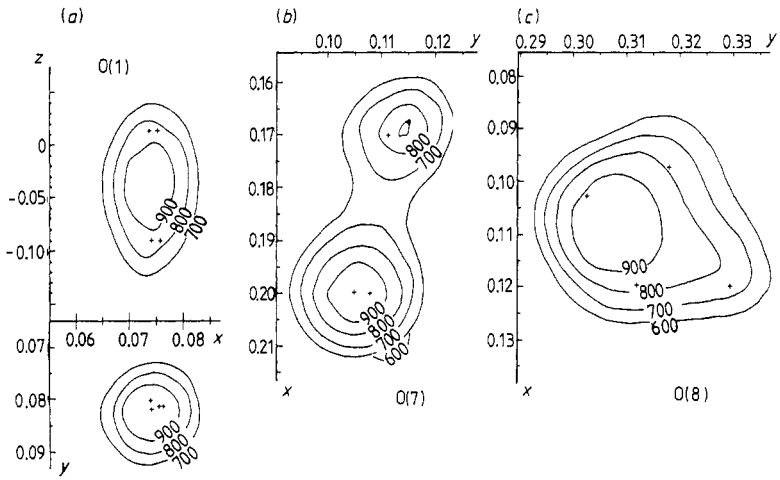

Figure 5. Observed electron density around the expected positions of three oxygen atoms in the mean structure. The sign + shows the positions of the actual pseudo-equivalent atoms (table 3) reduced to the mean structure. (*a*) O(1): the contour lines reveal only two oxygen positions along Oz. (*b*) O(7): the contour lines reveal only two positions in (xOy). (*c*) O(8): the contour lines now reveal four oxygen positions in (xOy).

4.3. Superstructure refinement

Several tests on the actual structure have been made according to the atomic positions derived from the mean structure, taking into account splittings and geometrical constraints arising from the symmetry and the tilting of octahedra chains. The most suitable and sensitive element, for testing the starting model of the actual structure and controlling the refinements, is indeed the calculated and observed intensities fit of the superstructure reflections. Thus, by trial and error methods, a model of the true structure can be derived; for instance, if we look at the Ba(11) and Ba(12) atoms, the x-splitting in the mean structure is noticeable, the z-coordinate values of these atoms can be, in a

given host lattice, unambiguously determined. To give an origin to the whole structure along the polar axis $\boldsymbol{c}$, the Ba(11) z-coordinate was fixed to 0.25.

We now point out the specific features of the procedure used for the refinement.

(*a*) A single scale factor was used in connecting F (observed) and F (calculated) for all the reflections. In the last refinements, the scale factor was calculated by least squares for each family of reflections, the atomic parameters being fixed; the corresponding values are statistically the same, showing that SR1 and SR2 intensities are not weakened in comparison with BR intensities and so, if disorder phenomena are involved, the corresponding effect should be negligible in establishing the actual structure.

(*b*) The four atomic groups, pseudo-equivalent through the $\mathbf{0}, \frac{1}{2}\boldsymbol{c}, \frac{1}{4}\boldsymbol{a} + \frac{1}{2}\boldsymbol{b}$ and $\frac{1}{4}\boldsymbol{a} + \frac{1}{2}\boldsymbol{b} + \frac{1}{2}\boldsymbol{c}$ vectors, were alternately refined in order to attenuate correlation effects. If the 140 β_{ij} of all the atoms are refined simultaneously, we observe 66 correlation coefficients $\rho\alpha\beta > 0.5$, including 14 $\rho\alpha\beta > 0.90$.

(*c*) The Nb, Na and Ba starting anisotropic thermal motion factors were set to their mean structure values, also taking into account the splitting. The thermal motion of the oxygen atoms was assumed isotropic.

(*d*) If the classical weighting scheme, derived from counting statistics, is introduced, there is no convergence of the z-coordinates; in successive cycles, all the z-shifts are of the same sign. This last point induced us to give an arbitrarily greater weight to SR1 and SR2, leaving a classical weighting scheme for the BR. Then, in the next refinement process, it is observed for the z-shifts, of both negative and positive signs. All parameters then converge, but slowly. In the final least-squares refinement, most of the Δ/σ values are less than 0.10, in particular this is the case for all the β_{ij}. The largest value is 0.33 (xNb41), two are about 0.20 and 13 between 0.10 and 0.20.

(*e*) Attempts to refine the site occupation ratio (Na/Ba) in the perovskite cages produced no significant changes, and the crystal structure analysis is thus consistent with the chemical analysis, and inconsistent with the presence of cation ordering.

(*f*) The residual electronic density in a full difference-series shows peaks less than 1 electron Å^{-3}.

4.4. Absolute configuration and single ferroelectric domain state

In principle, the investigated crystal was made into a single ferroelectric domain by electrical poling. In consequence, one can try to determine the absolute configuration of the structure, that is the absolute orientation of the atomic shifts parallel to $\boldsymbol{c}$. In this

Table 2. The seven reflections with maximal anomalous dispersion.

h	k	l	F_o	$\lvert F_i \rvert$	$\lvert F_l \rvert$	$r = \dfrac{\lvert F_i \rvert - \lvert F_l \rvert}{[\lvert F_i \rvert + \lvert F_l \rvert]/2}$
18	1	4	47.5	45.9	21	0.74
2	9	4	45.5	46.6	22	0.72
0	4	4	22.6	22.0	10.3	0.72
6	23	2	38.0	38.6	21.1	0.59
2	9	8	71.3	66.1	41.8	0.45
0	24	4	48.4	47.3	31.5	0.40
18	17	4	62.1	64.9	45.8	0.34

Table 3. Positional and thermal parameters with ESDs.

	x	*y*	*z*	*B*
Nb(11)	0.00073(3)	0.0	0.00926(9)	0.36(2)
Nb(12)	−0.00025(3)	0.0	0.50696(9)	0.36(2)
Nb(21)	−0.00027(3)	0.5	0.00588(9)	0.34(2)
Nb(22)	0.00030(3)	0.5	0.50579(9)	0.32(2)
Nb(31)	0.09005(2)	0.10861(5)	0.00505(6)	0.33(2)
Nb(32)	0.09168(5)	0.10839(5)	0.50649(6)	0.36(2)
Nb(33)	0.34177(2)	0.60823(5)	0.00510(6)	0.37(2)
Nb(34)	0.34051(2)	0.60805(5)	0.50379(6)	0.34(2)
Nb(41)	0.19595(2)	0.18336(4)	0.00609(6)	0.31(2)
Nb(42)	0.19527(2)	0.18068(4)	0.50681(6)	0.28(2)
Nb(43)	0.44570(2)	0.68216(5)	0.00245(6)	0.38(2)
Nb(44)	0.44654(2)	0.68188(5)	0.50486(6)	0.38(2)
Na(1)	0.125	0.25	0.24961(70)	0.85(11)
Na(2)	0.125	0.25	0.75199(70)	0.85(11)
Na(3)	0.37485(3)	0.75052(7)	0.24563(100)	0.82(11)
Ba(11)	0.00242(1)	0.17371(2)	0.25	0.85(1)
Ba(12)	−0.00513(1)	0.16921(2)	0.74843(10)	0.80(1)
Ba(21)	0.16367(1)	0.0	0.24639(12)	0.87(2)
Ba(22)	0.16378(1)	0.0	0.74996(13)	0.87(2)
Ba(23)	0.41335(1)	0.5	0.24853(15)	0.92(2)
Ba(24)	0.41454(1)	0.5	0.74905(15)	1.07(2)
O(11)	0.0370(1)	0.0802(3)	−0.0451(7)	0.58(7)
O(12)	0.0372(2)	0.0838(4)	0.5050(5)	0.52(8)
O(13)	0.2877(2)	0.5812(4)	0.0055(5)	0.53(8)
O(14)	0.2880(1)	0.5809(3)	0.4546(7)	0.69(7)
O(21)	0.1077(3)	0.0	−0.0098(8)	0.81(16)
O(22)	0.1069(2)	0.0	0.4631(11)	0.64(9)
O(23)	0.3583(3)	0.5	−0.0165(10)	1.14(15)
O(24)	0.3583(3)	0.5	0.5001(8)	0.50(12)
O(31)	0.0002(1)	0.2834(4)	−0.0319(7)	0.76(7)
O(32)	0.0004(2)	0.2850(4)	0.5038(5)	0.61(8)
O(41)	0.0723(1)	0.2141(4)	−0.0451(9)	1.16(8)
O(42)	0.0738(2)	0.2157(5)	0.4972(6)	0.85(11)
O(43)	0.3218(2)	0.7140(6)	−0.0128(6)	1.08(12)
O(44)	0.3215(2)	0.7138(4)	0.4651(8)	0.99(8)
O(51)	0.1080(1)	0.3546(4)	0.0091(6)	0.47(8)
O(52)	0.1069(1)	0.3592(3)	0.4480(8)	0.93(8)
O(53)	0.3570(2)	0.8537(5)	0.0062(7)	0.99(11)
O(54)	0.3572(1)	0.8562(3)	0.4516(8)	0.71(7)
O(61)	0.0410(2)	0.4247(5)	−0.0037(5)	0.70(10)
O(62)	0.0396(2)	0.4249(4)	0.4676(8)	1.01(8)
O(63)	0.2907(1)	0.9247(3)	−0.0348(7)	0.58(6)
O(64)	0.2911(2)	0.9262(5)	0.4881(6)	0.88(12)
O(7A1)	0.0836(1)	0.1146(3)	0.2329(10)	1.24(7)
O(7A2)	0.3348(1)	0.6116(3)	0.7343(10)	1.16(7)
O(7B1)	0.1003(1)	0.1053(3)	0.7329(9)	0.97(6)
O(7B2)	0.3498(1)	0.6079(3)	0.2334(11)	1.25(7)
O(8A1)	0.0513(1)	0.3028(3)	0.2310(9)	1.02(6)
O(8A2)	0.2984(1)	0.8184(3)	0.2359(11)	1.37(7)
O(8B1)	0.0598(1)	0.3302(3)	0.7331(9)	1.19(6)
O(8B2)	0.3097(1)	0.8126(3)	0.7322(10)	1.48(8)
O(91)	0.0085(1)	0.0	0.2328(12)	0.87(9)
O(92)	−0.0078(2)	0.0	0.7347(15)	0.87(8)
O(101)	0.2548(2)	0.0	0.2359(20)	1.43(11)
O(102)	0.2449(2)	0.0	0.7356(15)	1.36(11)

view, we observed that, about 600 (hkl) reflections are strongly affected by anomalous dispersion since their relative difference

$$r = \frac{|F(hkl)| - |F(hk\bar{l})|}{(|F(hkl)| + |F(hk\bar{l})|)/2}$$

was greater than 0.05. Accordingly, we gave a high weight to these reflections and a unitary weight to all the others. After the two refinements, we obtained the values $R_w(hkl) = 0.0437$ and $R_w(hk\bar{l}) = 0.0427$. The second value seemed significant and we retained $(hk\bar{l})$ as measured reflections. Table 2 shows for the highest r-values the good agreement between F_o and $|F_{\bar{l}}|$ calculated from the second refinement and gives comparatively the corresponding $|F_l|$ values. The fit, obtained with the results of the first refinement are clearly less good. The final atomic coordinates and the thermal parameters, with their standard deviations, are collected in table 3 and the characteristics of the vibration ellipsoids in table 4.

Finally, we verified, with these results, the single ferroelectric domain character of our crystal. If 180° ferroelectric domains are present in the crystal, denoting $\beta(\beta < \frac{1}{2})$ the proportion of one domain type, we have $I_{obs} = (1 - \beta)I_{hk\bar{l}} + \beta I_{hkl}$. Writing F_o and F_c at the same scale, we have, $F_o^2 - |F_c(hk\bar{l})|^2 = \beta[|F_c(hkl)|^2 - |F_c(hk\bar{l})|^2]$ or $y_j = \beta x_j$. Hence, the quantities y_j and x_j should be correlated with a correlation coefficient defined by

$$\rho = X_j Y_j / (\Sigma X_j^2)^{1/2} (\Sigma Y_j^2)^{1/2}$$

with $X_j = x_j - \langle x_j \rangle$ and $Y_j = y_j - \langle y_j \rangle$. We find $\rho \sim 0$ and $\beta \sim 0$ showing that the crystal is, to a good approximation, a single ferroelectric domain.

5. Description of the structure

A (001) projection of the actual structure of BNN, limited to one layer of NbO_6 octahedra (figure 6) illustrates the direction of the tilting and the connection of the chains.

5.1. Atomic pseudo-symmetrical scheme

(*a*) The BNN structure shows a noteworthy tetragonal local pseudo-symmetry in connection with a glide $(\boldsymbol{t} = \frac{1}{8}\boldsymbol{a} + \frac{1}{4}\boldsymbol{b})$ mirror $(2\bar{1}0)$ crossing the $\frac{1}{8}, 0, 0$ point. This pseudo-symmetry occurs especially for the Nb atoms and the oxygen atoms with z close to 0 and 0.5. This property is in agreement with the tetragonal pseudo-symmetry pointed out for the basic reflections and the existence of 90° ferroelastic domains often observed in the crystals.

(*b*) The $\frac{1}{4}\boldsymbol{a} + \frac{1}{2}\boldsymbol{b}$ and $\frac{1}{4}\boldsymbol{a} + \frac{1}{2}\boldsymbol{b} + \frac{1}{2}\boldsymbol{c}$ vectors are indeed nearly lattice vectors especially for the atoms previously mentioned. This property would explain how discommensuration walls [7] can be inserted between commensurate domains in the crystals.

5.2. Oxygen framework

The O—O distances, inside NbO_6 octahedra, show three main features.

(*a*) As previously pointed out, the octahedra are not regular and so, inside each of them, the dispersion of O—O distances is large; in the range 2.60(1)–2.95(1)Å.

Table 4. Thermal vibration features: magnitudes $u = \langle u^2 \rangle^{1/2}$ and direction cosines α_x, α_y, α_z of ellipsoid axes.

	u (Å)	α_x	α_y	α_z		u (Å)	α_x	α_y	α_z
Nb(11)	0.075(5)	0.359	0.0	0.933	Nb(44)	0.076(4)	0.807	0.361	−0.467
	0.063(5)	0.0	1.0	0.0		0.063(4)	0.308	−0.932	−0.188
	0.065(5)	0.933	0.0	−0.359		0.070(5)	0.503	−0.008	0.864
Nb(12)	0.079(5)	0.579	0.0	0.815	Na(1)	0.114(7)	0.997	0.078	0.0
	0.061(3)	0.0	1.0	0.0		0.085(12)	0.078	−0.997	0.0
	0.063(6)	0.815	0.0	−0.579		0.115(15)	0.0	0.0	1.0
Nb(21)	0.073(8)	0.571	0.0	0.821	Na(2)	0.105(8)	0.829	−0.559	0.0
	0.066(3)	0.0	1.0	0.0		0.087(11)	0.559	0.829	0.0
	0.060(10)	0.821	0.0	−0.571		0.123(14)	0.0	0.0	1.0
Nb(22)	0.068(6)	0.298	0.0	0.955	Na(3)	0.129(12)	0.170	−0.378	0.910
	0.071(3)	0.0	1.0	0.0		0.081(10)	0.829	−0.445	−0.339
	0.055(7)	0.955	0.0	−0.298		0.103(9)	0.533	0.812	0.237
Nb(31)	0.081(3)	0.117	−0.992	0.052	Ba(11)	0.143(1)	0.961	−0.266	0.080
	0.052(4)	0.749	0.054	−0.660		0.087(1)	0.278	0.913	−0.299
	0.065(4)	0.651	0.117	0.750		0.090(1)	0.006	0.307	0.952
Nb(32)	0.075(4)	0.004	−0.850	−0.527	Ba(12)	0.139(1)	0.986	0.126	−0.108
	0.059(3)	0.979	0.111	−0.171		0.084(1)	0.066	−0.896	−0.438
	0.068(5)	0.205	−0.515	0.823		0.088(1)	0.152	−0.425	0.892
Nb(33)	0.073(4)	0.677	−0.317	−0.664	Ba(21)	0.092(2)	0.996	0.0	−0.088
	0.064(4)	0.672	0.634	0.382		0.162(2)	0.0	1.0	0.0
	0.069(5)	0.300	−0.705	0.643		0.078(4)	0.088	0.0	0.996
Nb(34)	0.073(3)	0.357	0.920	−0.163	Ba(22)	0.092(3)	0.170	0.0	0.958
	0.059(5)	0.604	−0.094	0.791		0.153(1)	0.0	1.0	0.0
	0.064	0.712	−0.381	−0.590		0.083(2)	0.985	0.0	−0.170
Nb(41)	0.075(2)	0.965	−0.167	−0.202	Ba(23)	0.092(3)	0.911	0.0	−0.412
	0.055(5)	0.087	0.930	−0.358		0.163(2)	0.0	1.0	0.0
	0.060(5)	0.247	0.328	0.912		0.084(4)	0.412	0.0	0.911
Nb(42)	0.078(3)	0.840	0.380	0.388	Ba(24)	0.091(2)	0.979	0.0	−0.205
	0.038(8)	0.076	0.626	−0.776		0.204(2)	0.0	1.0	0.0
	0.071(4)	0.538	−0.681	−0.496		0.086(4)	0.205	0.0	0.979
Nb(43)	0.077(4)	0.999	0.013	0.037					
	0.061(4)	0.015	−0.997	−0.072					
	0.070(5)	0.034	0.074	−0.997					

(*b*) Inside each octahedron, one or two O—O distances about 2.65 Å, shorter than the others are systematically found. In all the octrahedra (oct. 1), where Nb takes a general position, and which are used in building the perovskite cages, only one short edge is involved and it belongs to one of the adjacent pentagonal cages. In all the octahedra (oct. 2), where Nb is in an m mirror, and is binding four perovskite arrangements, two short opposite edges are found belonging to adjacent pentagonal cages. These short O—O distances are obvious from figure 6.

(*c*) The distortion of the two sorts of octahedra is well understood considering the three O—O distances of the diagonals inside each of them: in all the oct. 1, one diagonal, almost in the (001) plane is systematically shorter (3.87–3.89 Å) than the two others

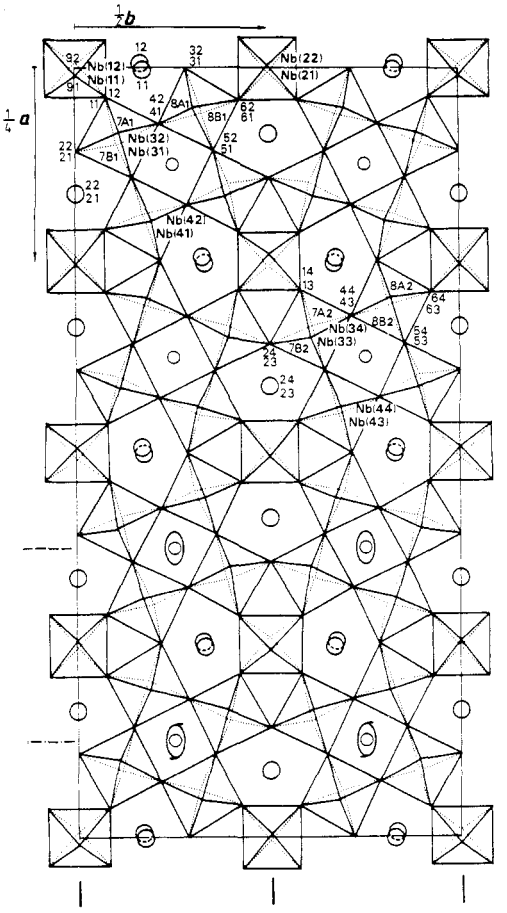

Figure 6. Projection (001) of the actual structure of BNN. Only a slice of NbO_6 octahedra is drawn ($-0.3 < z < +0.3$). The atom numbers are related to those of the mean structure (figure 1): thus Nb(3) in the mean structure corresponds to the four atoms Nb(31), Nb(32), Nb(33) and Nb(34) of the actual structure through $\mathbf{0}$, $\frac{1}{2}\boldsymbol{c}$, $\frac{1}{4}\boldsymbol{a} + \frac{1}{2}\boldsymbol{b}$, $\frac{1}{4}\boldsymbol{a} + \frac{1}{2}\boldsymbol{b} + \frac{1}{2}\boldsymbol{c}$. The elements of the space group B*b*m2 are drawn in the lower part of the figure.

(3.98–4.05 Å), when in all the oct. 2, the two diagonals, almost in the (001) plane are systematically shorter (3.87–3.95 Å) than the third one (4.00–4.05 Å), giving for them a lengthening in a direction close to [001]. A similar effect is involved in the tetragonal ferroelectric phase of $BaTiO_3$ [11]. Indeed, inside TiO_6 octahedra, the O—O diagonal distance (~4.04 Å) in the spontaneous polarisation direction is a little larger than the other diagonal distances (3.99 Å).

5.3. Arrangement of the octahedra NbO_6

An attractive manner of describing the BNN structure is to consider it as being built with units (Nb_5O_{24}) of five octahedra sharing corners (figure 7). Each of these units involves two sets of three consecutive O—O short distances turned toward the pentagonal tunnels. Actually, four independent units of this type exist, but because of the pseudo-

symmetry, only two different units are found, bound with two oxygen atoms. These ones differ only by the orientation and the amplitude of the tilt of the central octahedron (figure 7) which induces the tilted orientation of the four others.

5.4. Tilting and shearing of NbO_6 octahedra

We define arbitrarily the tilting angle t inside each octahedron as the angle between the normal N to the mean plane, determined by a least-squares fit involving the four oxygen atoms with $z \sim 0$ (or $z \sim 0.5$), and the normal N_0 to (001) plane. The shearing angle s is defined as the angle between N and the vector S connecting the two oxygen atoms on both sides of the mean plane (figure 7). With regard to octahedra (oct. 2) where Nb is

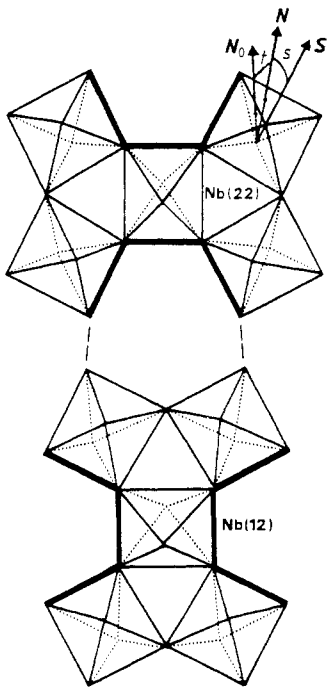

Figure 7. The two different units (Nb_5O_{24}) found in BNN. The bold lines are the systematically short O—O distances.

in a mirror m, only one rotation—angle t—defines the tilting, around Oy, that is an axis crossing the middle of the two opposite sides of the octahedron, while in the other octahedra (oct. 1), two rotation angles of this type, t_1 and t_2, around two perpendicular axes should be introduced: t_1 and t_2 correspond to rotations around the Ox' and Oy' axes, respectively, obtained from Ox and Oy through a rotation of 30° (clockwise) around z.

The calculated values (table 5) show that, apart from $Nb(33)O_6$, one of the rotations t_1 or t_2 is favoured. The corresponding values of t and s point out that tilting and shearing are both involved in all the octahedra but the tilting effect is clearly predominant.

Table 5. Tilting (t) and shearing (s) angles (in degrees) of NbO_6 octahedra.

	t_1	t_2	t	s
Nb(11)	0.0	8.7	8.7	0.6
Nb(12)	0.0	−8.6	−8.6	0.6
Nb(21)	0.0	−4.9	−4.9	0.0
Nb(22)	0.0	3.3	3.3	1.7
Nb(31)	2.1	−7.2	7.5	1.2
Nb(32)	−2.2	7.3	7.6	0.9
Nb(33)	−4.5	4.5	6.4	2.9
Nb(34)	1.8	−6.9	7.2	1.0
Nb(41)	−6.6	−0.5	6.6	1.8
Nb(42)	7.0	−1.6	7.2	1.7
Nb(43)	2.5	−6.1	6.6	0.9
Nb(44)	−1.4	4.9	5.1	1.0

5.5. Bond distances Nb—O, Na—O, Ba—O

(*a*) *Nb—O bonds.* Inside each octahedron there are three types of Nb—O bonds. (i) Mean strength bonds, perpendicular to the ferroelectric shift of the Nb atoms, with Nb—O distances in the range 1.94–2.02 Å. (ii) Parallel to the Nb shifts, there are strong bonds and relaxed ones, with Nb—O distances respectively equal to about 1.84 and 2.19 Å. Note that the mean value of the last two average distances (1.835 and 2.188 Å) does not coincide exactly with the average of the third, intermediate, distance (1.98 Å). This effect must be related to the lengthening of the octahedra already discussed.

(*b*) *Ba—O bonds in the pentagonal tunnels.* Only the Ba atoms are enclosed in the pentagonal tunnels. Each Ba is surrounded by 15 oxygen atoms considered as first neighbours. The Ba—O distances show a great dispersion, the shortest value being 2.64 Å, but no discontinuity, so that a coordination number cannot be given with certainty to Ba inside its site. Note that the Ba coordination numbers considered by Shannon [12] range from 6 to 12.

(*c*) *A—O bonds in the perovskite cages.* The mixed sites Na/Ba are statistically distributed over all the perovskite cages; the proportion of Ba/Na atoms being close to 10%. Each Na is bonded to 12 oxygen atoms, the Na—O distances (table 6) being distributed around the mean value 2.78 Å in the range 2.541(7)–3.162(7) Å and the polyhedron shape is a distorted cubo-octahedron. It is noted that the first distance Na—O (2.54 Å) is greater than the shortest Na—O distance (2.38(3) Å) observed in the distorted perovskite structure of $NaNbO_3$ [13] where Na also has coordination 12.

Each perovskite cage is bounded by six windows limited by four oxygen atoms. In the [001] direction, the window shape is nearly square (figure 6) for each cage with diagonal about 2.95 Å. In the two other directions of the cage, the windows are rather diamond shaped and the little diagonal ranges from 2.55 to 2.75 Å, which makes a possible migration of Na^+ ions by this route unlikely.

The minimal A—O distances observed in these cages (2.54–2.57 Å) are rather unusual in the case of barium. Actually, in the tetragonal $BaTiO_3$ phase [11], the shortest distance Ba—O is 2.798 Å inside the perovskite cage. The ability of barium to form

Table 6. Na—O distances (Å).

Na(1)—O(41)	2 × 3.060(7)	Na(2)—O(41)	2 × 2.541(7)
Na(1)—O(42)	2 × 2.742(7)	Na(2)—O(42)	2 × 2.783(7)
Na(1)—O(51)	2 × 2.727(7)	Na(2)—O(51)	2 × 2.822(7)
Na(1)—O(52)	2 × 2.572(7)	Na(2)—O(52)	2 × 3.162(7)
Na(1)—O(7A1)	2 × 2.797(5)	Na(2)—O(7B1)	2 × 2.698(5)
Na(1)—O(8A1)	2 × 2.759(4)	Na(2)—O(8B1)	2 × 2.698(4)
Na(3)—O(43)	2.854(8)	Na(3)—O(54)	2.561(8)
Na(3)—O(43)	2.761(6)	Na(3)—O(54)	3.073(8)
Na(3)—O(44)	2.647(9)	Na(3)—O(7A2)	2.814(5)
Na(3)—O(44)	2.995(9)	Na(3)—O(7B2)	2.663(5)
Na(3)—O(53)	2.711(9)	Na(3)—O(8A2)	2.943(4)
Na(3)—O(53)	2.846(9)	Na(3)—O(8B2)	2.557(4)

iono-covalent Ba—O bonds with a σ character [14] may favour the shortest Ba—O distances observed in BNN. The contribution of this cation to the ferroelectricity in this phase, characterised by its significant displacement inside its polyhedron in the perovskite cages as well as in the pentagonal tunnels, is supported by this σ character.

5.6. Cation shifts in connection with ferroelectricity

The cation shifts are defined through the vectors ***GC*** where ***C*** is the cation position inside its polyhedron with centre ***G***, calculated from all the first-neighbour oxygen atoms; six for Nb, 12 for Na and 15 for Ba. All the cations, including Na and Ba, display shifts along *z* of the same positive sign. This effect is illustrated in figure 8 for the Nb atoms for which all the *z* components of the shifts (Δ_z) are very close to their mean value 0.196 Å. The use of the empirical relationship [15] involving only the Nb displacement lead to T_c = 768 K, slightly less than the measured value of 825 K.

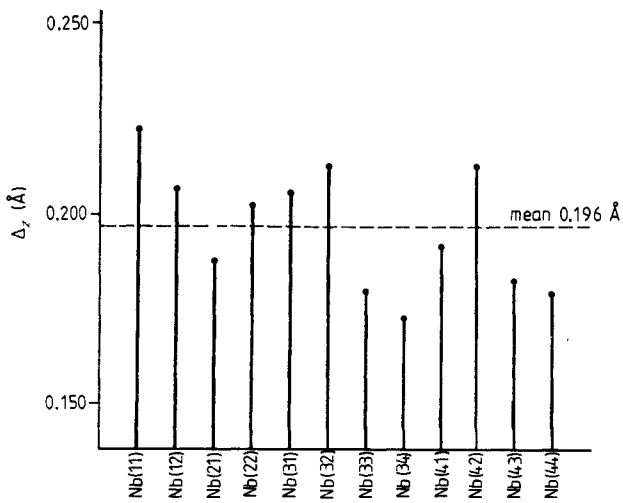

Figure 8. Shift (Å) of Nb atoms in each NbO_6 octahedron.

In comparison, the shift amplitudes of Na and Ba atoms along z are less, the mean values being equal to 0.158 and 0.140 Å respectively. The shift components x and y are negligible for Nb and Na atoms and noticeable for Ba atoms.

From the elementary dipole moment calculation it is easy to predict the approximate size of the spontaneous polarisation P_s, far from the transition temperature. It results in a value P_s equal to 30 $\mu C\,cm^{-2}$ to be compared with the measured value at room temperature of 40 $\mu C\,cm^{-2}$ [16].

6. Discussion and conclusion

The mean structure determined here confirms the main features of the one determined by Jamieson *et al*, in particular the existence of split positions for a certain number of atoms as well as the order of magnitude of the splittings. Our results also improve the precision with which the characteristics of the mean structure is known. They show that the origin of the observed splittings resides essentially in rotations of the various Nb—O_6 octahedra, and secondarily in a shearing of these octahedra. They also reveal a small feature, consistent with the former mechanism: a splitting of certain atoms into four atomic positions instead of two (figure 5). This feature had escaped the earlier investigation. In agreement with this more detailed description of the mean structure, we obtain a reliability factor of 0.039, significantly smaller than the factor of 0.058, achieved by the structural refinement performed by Jamieson *et al*.

The structure of the commensurate, room temperature, phase of BNN has been determined for the first time on the basis of x-ray diffraction. Our results bring a quantitative confirmation to the correctness of the space group B*b*m2 assigned to this structure. They also agree with previous inferences which had assumed that the differences between the distorted structure of BNN and the reference tetragonal tungsten-bronze structure reside mainly in a collective displacement of the atoms forming the oxygen octahedra. We have specified the detailed characteristics of the rotations and the shears experienced by each oxygen octahedron in the structure. This set of distortions constitutes the nature of the modulation existing in BNN. Indeed though the room temperature structure involves a quasi-commensurate modulation, it is likely that, in its incommensurate state, the modulation will comprise the same type of atomic displacements. In view of our results we can see that the modulation is associated with the displacement of all the atoms giving rise to split positions in the mean structure. Moreover, we can assert that the modulation is mainly of the displacive type since the actual structure does not contain split atomic positions. This displacive character was previously identified on the basis of inelastic neutron scattering results showing the existence of a soft mode above the transition giving rise to the modulated structure.

The validity of our approximation, neglecting the weak incommensurability ($\delta = 0.01$) can be stated from HREM observations [18]. Actually, these observations point out that the quasi-commensurate phase of BNN consists of commensurate (~500 Å) regions separated by thin discommensuration walls (soliton regime). Assuming no alteration of the satellite intensities, the result of our work should give the right amplitudes of the atomic displacements only inside the commensurate regions without any information about the walls.

Finally, it is worth pointing out that the value of the reliability factor for the actual structure ($R_{tot} = 0.031$) shows the validity of the adoption of a commensurate unit cell to describe the structure of the quasi-commensurate phase of BNN.

References

[1] Tolédano J-C 1975 *Phys. Rev.* B **12** 943
[2] Schneck J and Denoyer F 1981 *Phys. Rev.* B **23** 383
[3] Schneck J, Tolédano J-C, Errandonea G, Litzler A, Savary H, Manolikas C, Kiat J-M and Calvarin G 1987 *Phase Transitions* **9** 359
[4] Errandonea G, Tolédano J-C, Litzler A, Savary H, Schneck J and Aubrée J 1984 *J. Phys. Lett.* **45** L329
[5] Schneck J, Tolédano J-C, Joffrin C, Aubrée J, Joukoff B and Gabelotaud A 1982 *Phys. Rev.* B **25** 1766
[6] Tolédano J-C, Errandonea G, Schneck J, Litzler A, Savary H, Bonnouvrier F and Esteoule M-L 1985 *Japan. J. Appl. Phys.* **24** S24-2 290
[7] Van Tendeloo G, Amelincks S, Manolikas C and Wen Shulin 1985 *Phys. Status Solidi* **91** 483
[8] Jamieson P B, Abrahams S C and Bernstein J L 1969 *J. Chem. Phys.* **50** 4352
[9] Magneli A 1949 *Ark. Kemi* **1** 213
[10] Britton D 1972 *Acta Crystallogr.* A **28** 296
[11] Frazer B C, Danner H R and Pepinsky R 1955 *Phys. Rev.* **100** 745
[12] Shannon R D 1976 *Acta Crystallogr.* A **32** 751
[13] Sakowski-Cowley A C, Lukaszewicz K and Megaw H D 1969 *Acta Crystallogr.* B **25** 851
[14] Goodenough J B 1973 *Les Oxydes des Métaux de Transition* (Paris: Gauthier Villars)
[15] Abrahams S C, Kurtz S K and Jamieson P B 1968 *Phys. Rev.* **172** 551
[16] Wemple S H, DiDomenico M and Camlibel I 1968 *Appl. Phys. Lett.* **12** 209
[17] *International Tables of X-ray Crystallography* 1974 vol 4 (Birmingham: Kynock)
[18] Barré S, Mutka H and Roucau C 1988 *Phys. Rev.* **38** 9113